Soils and Foundations 2013;53(6):853–867

The Japanese Geotechnical Society

Soils and Foundations

www.sciencedirect.com
journal homepage: www.elsevier.com/locate/sandf

Vertical bearing capacity of tapered piles in sands using cavity expansion theory

Suman Manandhar[a,*], Noriyuki Yasufuku[b]

[a]*Institute of Lowland and Marine Research, Saga University, 840-8502 Saga, Japan*
[b]*Faculty of Civil Engineering, Kyushu University, 819-0395 Fukuoka, Japan*

Received 30 October 2012; received in revised form 4 July 2013; accepted 20 August 2013
Available online 22 November 2013

Abstract

On the basis of the mechanism of tapered piles and evidence obtained from small scale model tests, this paper proposes cylindrical and spherical cavity expansion theories to evaluate the skin friction by introducing a stress–dilatancy relationship, as well as the end bearing capacity of tapered piles by introducing a tapering factor. In general, in order to evaluate the skin friction, either the angle of internal friction or dilatancy angle is assumed to be constant. This research improves on this drawback and considers both properties to calculate the skin friction through an iterative process in the load transfer method. At the mean time, the effect of angle of tapering is introduced to evaluate the end bearing capacity of tapered piles. The test results and proposed models show that a slight increase in the tapering angle of the pile results in higher skin friction and affects the end bearing resistance compared with conventional straight piles on different types of sands at different relative densities. The proposed models are then applied to different types of prototype and real type pile tests in order to evaluate the predicted skin friction, expected end bearing capacity and vertical bearing capacity.

Keywords: Skin friction; End bearing capacity; Vertical bearing capacity; Cavity expansion theory; Tapered piles; Sands

1. Introduction

Tapered piles with a difference in axial diameter at their top and bottom have merits over conventional piles in terms of the bearing capacity and the radial stress. A small increase in the degree of tapering can achieve higher skin friction and affect the end bearing resistance. Dmokhovskii (1927) observed that the overall resistance of piles was increased by a factor of 5–9 when mobilised towards depth. However, there is a negligible taper on the lateral surface of the pile. In the meantime, when tapered piles are penetrated downward in a frictional mode, the mechanism demonstrates a good pressure effect on it (Manandhar et al., 2009a, 2009b). Further, Manadhar (2010), Manandhar et al. (2010a, 2010b) found that tapering and wedging effects are responsible for increasing the normalised skin friction and normalised horizontal stresses. Yet in practice, very few researchers have been carrying out research on tapered piles, which may be due to a lack of awareness of their basic existence together with a lack of modern and reliable analytical methods for evaluating their bearing capacity (Horvath and Trochalides, 2004). Nevertheless, Norlund (1963) applied an analytical method in order to estimate the axial capacity of tapered piles when the tapered piles were driven into cohesionless soil, the accurate model was not well introduced in the context of deep foundation. A number of

*Corresponding author.
E-mail address: geosuman@gmail.com (S. Manandhar).
Peer review under responsibility of The Japanese Geotechnical Society.

Production and hosting by Elsevier

0038-0806
http://dx.doi.org/10.1016/j.sandf.2013.10.005

pioneering experts in geotech proposed theoretical methods using a cavity expansion theory (Vesic´, 1972; Baligh, 1976; Hughes et al., 1977; Yu and Houlsby, 1991). It has been found that the cavity expansion theory introduced by Yu and Houlsby (1991) is widely used by researchers due to its characteristics in evaluating large straining conditions, provides a complete solution for cylindrical cavity expansion in ideal elastic–plastic models in non-associated flow rule, and measures the most closed form solution (Kodikara and Moore, 1993). In general, one of the soil parameters, angle of internal friction or dilatancy angle is assumed to be constant for the ease of computing process. However, the stress–dilatancy relationship is an interdependent function of confining pressure, relative density and angle of internal friction. Therefore, the new concept is inserted to extend the idea proposed by Kodikara and Moore (1993) together with cavity expansion theory to evaluate the skin friction of tapered piles by introducing Bolton's (1986, 1987) stress–dilatancy equation. In the extended model, the increase of confining pressure will increase relative density along with an increase in the angle of internal friction and dilatancy. All these parameters are successfully inserted in Yu and Houlsby's (1991) cavity expansion solution and computed at each segment of the pile (Manandhar, 2010; Manandhar and Yasufuku, 2011b).

Moreover, there have been a limited number of studies related to the influence of tapering on an end bearing mechanism (Manandhar and Yasufuku, 2011a). Evidence derived from prototype model tests reported by Sakr et al. (2004) in the laboratory showed significant tapering effects on end bearing capacity even though the tapering angle is increased in small fractions. Very few researchers have noticed that the end bearing capacity is increased by tapered piles. In this regard, the research has been further assessed so as to introduce the tapering angle of the pile in the previously established analytical spherical cavity expansion theory with the aim of evaluating the end bearing capacity of non-displacement cylindrical piles in closed forms (Yasufuku and Hyde, 1995; Yasufuku et al., 2001). Hence, the model is advanced by inserting the tapering angle of the pile to measure the effects on end bearing capacity.

2. Mobilised mechanism of skin friction and end bearing capacity

When the pile is mobilised downward in a frictional mode, the failure zone developed along the soil–pile interface partly causes the surface to bulge up to certain depths. Furthermore, horizontal displacement occurs below the critical depth when the soil is compressed elastically and partly consolidated around the interface. A medium dense sand shows that a thin layer of soil particles drag along and compress the layers along lateral directions. Kézdi (1975) noticed that the diameter of the disturbed zone was approximately six times the diameter of the pile in which the displacements had decreased according to parabolic law. Besides, the failure zone exceeds below the tip of the pile when the angle of tapering is changed (Manandhar and Yasufuku, 2011b). In order to understand the mobilised mechanism, the smallest model pile testing was performed with different types of tapered piles in dense sand.

Three steel chromium piles—one straight (S') and two tapered (T_1' and T_2')—with the same pile tip diameter and length were considered for the pile loading test (Table 1). The pile load chamber has dimensions of 460 mm height and 280 mm diameter as shown in Fig. 1(a). The cylindrical chamber has the merit of splitting the chamber into two halves to observe the mobilised mechanism of pile. A typical Toyoura sand (TO sand) was prepared at 80% relative density utilising the free fall method. One centimetre of each black-coloured soil was filled alternatively with non-coloured TO sand at the same density. Then the pile was installed at the centre of the chamber as a cast-in-place type. Then, layered modelled ground was prepared up to a depth of 400 mm and covered by an upper plate to furnish the overburden pressure. Since this is a very small model chamber, only 3.2 kPa overburden pressure can be applied. Then, piles were mobilised at a speed

Table 1
Geometrical configuration of different types of piles.

Types of Model Piles	Naming	L (mm)	D_t (mm)	d (mm)	α°	FRP reinforcement direction	Modulus of elasticity GPa
Smallest model steel piles	S'	345	13	13	0.00		2.0
	T_1'	345	20	13	0.70		2.0
	T_2'	345	28	13	1.40		2.0
Smaller model steel piles	S	500	25	25	0.00	na	2.0
	T-1	500	35	25	0.70	na	2.0
	T-2	500	45	25	1.40	na	2.0
Prototype FRP piles	FC	1524	168.3	168.3	0.00	na	31.86
	T-3	1524	170.0	198.0	0.53	0°	33.20
	T-4	1524	159.0	197.0	0.71	0°	33.15
	T-5	1524	155.0	215.0	1.13	0°	33.15

Note: L: length of pile; D_t: diameter at the pile head; d: pile tip diameter; FRP: fiber-reinforced polymer; α: angle of tapering; na: not applicable.

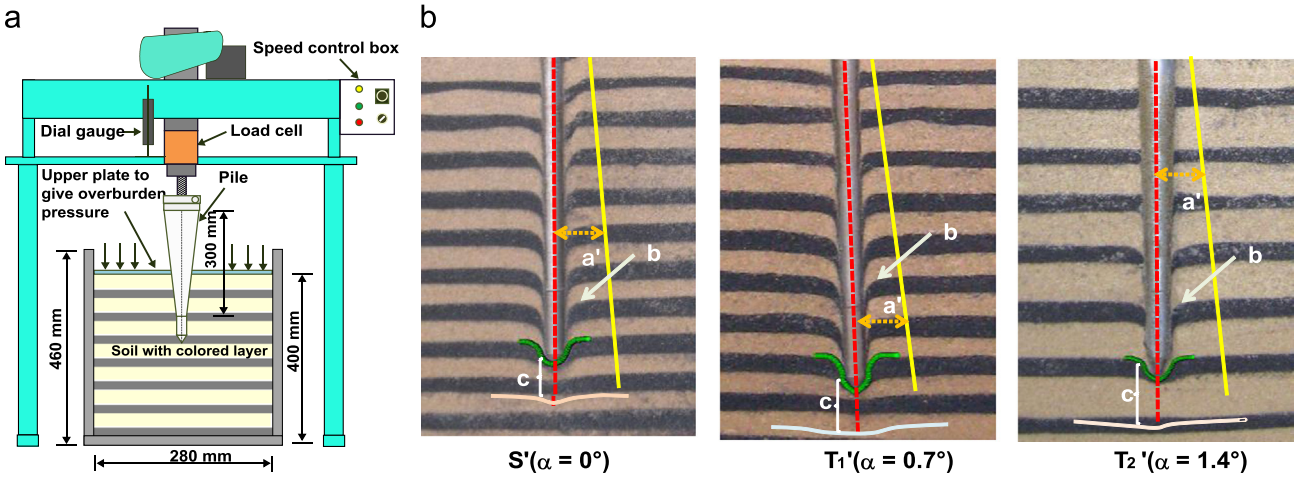

Fig. 1. (a) Schematic figure of smallest pile loading test (figure not to scale); (b) mobilised mechanism of pile: a′=effective length of influenced zone; b=convex heave due to effect of pile; c=effective length at the pile tip settlement.

of 4 mm/min up to a depth of 100 mm. After loading, the chamber was detached and immersed in the water bath for a couple of hours, following which half of the chamber was split up. Then, the modelled ground was easily trimmed to observe the mobilised mechanism carefully (Fig. 1(b)). Here, the chamber was submerged in the water bath to prevent failure of the soil specimen during splitting and trimming of the modelled ground.

2.1. Visual interpretation of skin friction and end bearing capacity

In this section, a visual inspection was carried out in the disturbed pile–ground interface around the chamber after trimming the soil. The failed zone is termed as the influence zone and the linear dimension of the disturbed region from the centre of the pile named as the radius of influenced zone. The radius of the affected area around the shaft of the pile was measured visually. The results showed that the tapered pile had a higher radius of influence compared to the straight pile, as shown in Fig. 1(b). The effect of the radius of influence area increases in line with increases to the angle of tapering. Moreover, it was found that the convex heave on the pile–ground interface had narrowed and decreased in the tapered piles. The reason for this mechanism is due to an increase in horizontal stresses with increases to the degree of tapering. All the measured maximum and minimum radiuses of influence of the pile–ground influenced area were measured and the mean of the influenced area was plotted for all three types of piles, as shown in Fig. 2. The most tapered pile considered for this experiment showed the highest radius of influence when compared to that of straight piles. This visual inspection gives strong evidence of increases in skin friction and radial stress and minimises the failure zone effectively through the tapered pile. The next section discusses a relatively larger model pile loading test, which supports the visual interpretation of skin friction and radial stresses of tapered piles of the smallest model pile loading tests. The mobilised mechanism of tapered piles does not only affect the shaft around the soil–pile interface, but also below the pile tip settlement. Fig. 3 shows the increment of failure mode measured from the pile tip to

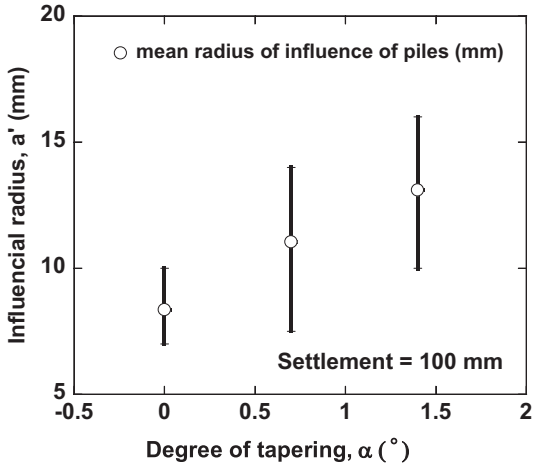

Fig. 2. Visually measured radius of influence of skin friction of piles.

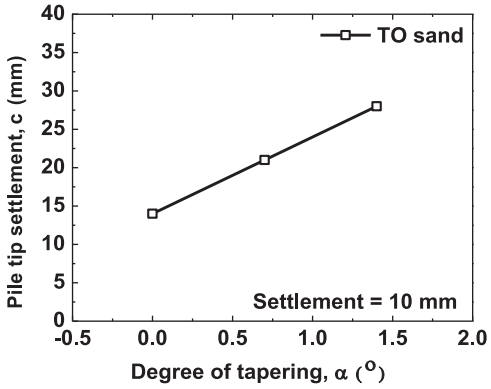

Fig. 3. Visually measured pile tip settlement.

the maximum curvature for all piles. Increases in tapering angle serve to increase the failure zone below the pile tip.

3. Benefits of tapered piles based on small model tests

In this section, air-dried typical TO sand was considered for model tests at 80% of relative density after determining the

Table 2
Index and strength parameters of different types of soil.

Descriptions	TO sand	K-7 sand	FB sand (Sakr et al. (2004, 2005, 2007)
Density of particles, ρ_s (g/cm^3)	2.65	2.62	2.68
Maximum density, ρ_{max} (g/cm^3)	1.64	1.60	1.772
Minimum density, ρ_{min} (g/cm^3)	1.34	1.19	1.466
Density at I_D 80%, ρ_{80} (g/cm^3)	1.58	1.52	na
Density at I_D 60%, ρ_{60} (g/cm^3)	1.52	1.43	na
Maximum void ratio, e_{max}	0.98	1.20	0.794
Minimum void ratio, e_{min}	0.62	0.64	0.484
Void ratio at I_D 90%, e_{90}	na	na	0.68
Void ratio at I_D 80%, e_{80}	0.68	0.73	na
Void ratio at I_D 60%, e_{60}	0.74	0.83	na
Effective grain size, D_{10} (mm)	na	na	0.14
Mean grain size, D_{50} (mm)	na	na	0.26
Uniformity coefficient, U_c	1.40	4.0	2.143
Coefficient of curvature, U'_c	0.86	1.21	0.905
Per cent fines, (%) F_c	1.10	14	na
Peak stress, ϕ (deg)	42.00	47.00	37.00
Critical stress state, ϕ'_{cv} (deg)	32.00	34.00	31.00 (assumed)

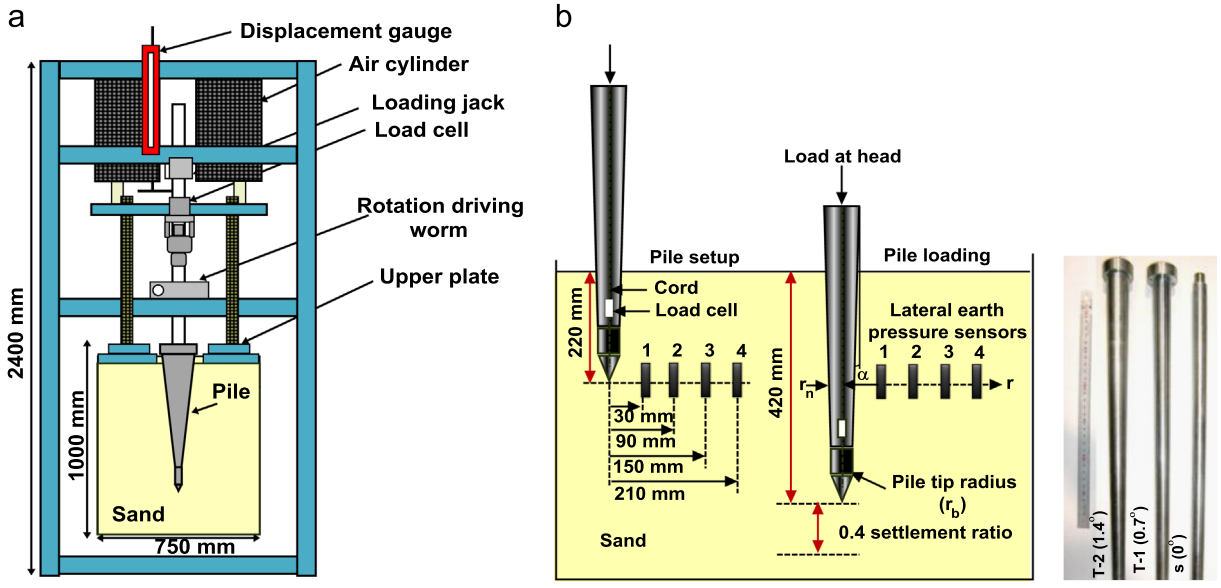

Fig. 4. Schematic figure of smaller pile loading apparatus, types of steel piles, and procedures of cast-in-place pile set up and loading (diagrams (a) and (b) not to scale).

maximum–minimum densities (Japan Geotechnical Society, 2009). The model ground was prepared using multiple sieving techniques (Miura and Toki, 1982). Chromium plated steel model piles with the same pile tip diameter (25 mm) and equal lengths (500 mm) were taken into consideration for experimental purposes. One straight (S) and two tapered (T1 and T2) piles having an angle of tapering of 0.7° and 1.4° were chosen, similar to the smallest model chamber testing. The only differences in these hollow types are the presence of load cells at the pile head and tip connected with a cord to measure the skin friction directly. The difference between the loads at the pile head and pile tip, gives the skin friction. Table 2 shows the fundamental parameters of soils and geometry of model piles. A typical pile loading apparatus which has dimensions of 1000 mm × 750 mm, and its arrangements are shown in Fig. 4. The overburden pressure was transferred through the upper plate to the model ground vertically. At first, the cylindrical chamber was almost completely filled with sand at an 80% relative density up to 710 mm from the bottom. Then, the pile was installed at the centre of the chamber. Four transducers at an equal interval of 60 mm from one to another were mounted to measure lateral earth pressures. The first transducer was set up near to the pile tip. From the centre, earth pressure sensors 1, 2, 3 and 4 were mounted at 30 mm, 90 mm, 150 mm, and 210 mm intervals respectively (Fig. 4). Afterwards, the chamber was filled up to 930 mm with soil to simulate cast-in-place conditions. Then, 50 kPa overburden pressure (σ_v) was furnished vertically. Initially, the pile was penetrated down up to

200 mm into the model ground at a rate of 5 mm/min and the stress was relaxed for up to fifteen hours. Finally, the pile loading test was carried out up to a 0.4 settlement ratio in which S and D are considered as settlement and pile tip diameter. During pile penetration, the normalised unit skin friction (f_s) is generally calculated by dividing the surface area of the pile to the skin friction, considering the average diameter of the pile head and tip. As Fig. 5 shows, the unit skin frictions of the most tapered pile increased more compared to that of a conventional straight cylindrical pile. Similarly, Fig. 6 shows that there is also an increase in normalised end bearing capacity of tapered piles. On the basis of these benefits of tapered piles, two different types of models are proposed to evaluate skin friction and end bearing capacity separately using cavity expansion theory.

3.1. Effects of lateral pressure

Radial distance from the centre of the pile was normalised by dividing the distance of transducers to the pile tip radius (r/r_n) to check the effect of lateral pressure by installing pressure cells in the ground from the centre of the pile. Then, the stress obtained during pile loading was carefully measured at 0.1 settlement ratios, since it is generally considered for the purpose of design (Fig. 4). Fig. 7 shows that near the pile–ground interface, the stresses are higher and reduced significantly from the centre of pile–ground interface. TO sand showed the highest radial stress governed at the pile–ground interface, which was more than 3 times when the most tapered pile T2 was penetrated at a 0.1 settlement ratio compared to

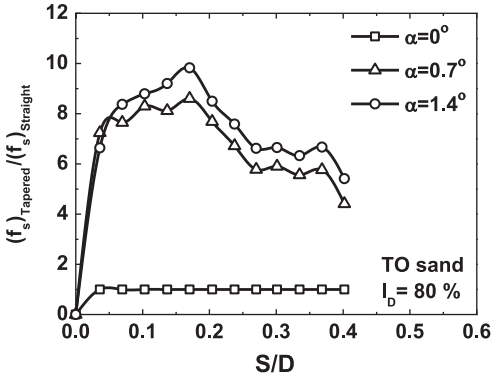

Fig. 5. Normalised unit skin friction ratios of TO sand.

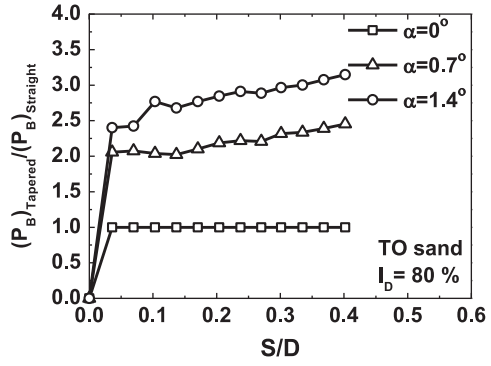

Fig. 6. Normalised end bearing capacity of TO sand.

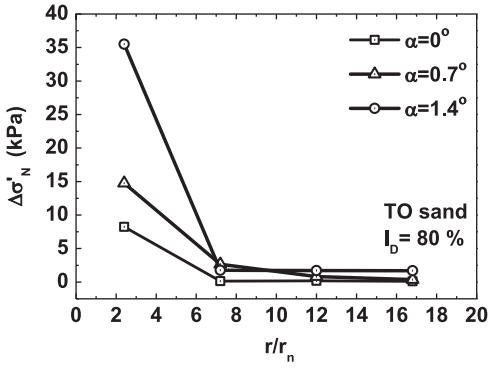

Fig. 7. Lateral stress distribution at 0.1 settlement ratio on TO sand.

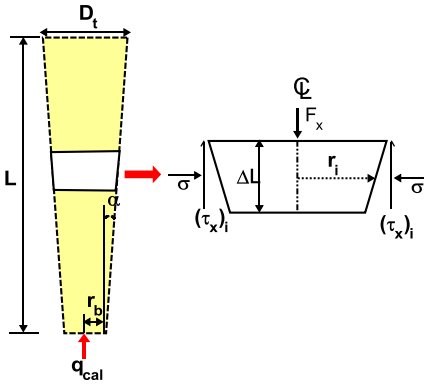

Fig. 8. Outline of evaluation of bearing capacity.

that of the straight cylindrical pile. Furthermore, the lateral earth pressure adjacent to the first earth transducer shows a sudden fall of lateral earth pressure and tends nearly to zero. However, it is very near to the centre of the pile. This may be an indication of the movement of a greater amount of soil particles towards the pile. It can be clearly seen that the normalised radial distance of tapered piles with angles from 0° to 1.4° is affected at least eight times from the centre of the pile. This mechanism strongly supports the smallest model tests in the previous section in understanding the mobilised mechanism and tapering effects.

4. Evaluation of total bearing capacity

The outline of total bearing capacity with settlement of the tapered pile can be generalised by summation of the total skin friction and the end-bearing capacity by multiplying their corresponding surface area and cross-sectional area (Fig. 8), which can be expressed with the following formula:

$$P_T = P_S + P_B \tag{1}$$

where P_T is the total bearing capacity of the tapered pile, P_S and P_B are total skin friction and total pile tip resistance.

In general, the skin friction, P_S and the tip resistance P_B in kN can be expressed with the following formula:

$$P_T = \sum_{i=1}^{n} (\tau_x)_i \, 2\pi r_i \Delta L + q_{cal} \, \pi r_b^2 \tag{2}$$

where $(\tau_x)_i$ is the vertical shear stress of the embedded pile section of each incremental length ΔL having radius r_i at each

segment measured from the mid-point of the pile, q_{cal} is the end bearing capacity and r_b is the radius of the pile tip.

The experimental evidence showed that the maximum tapered pile increased the compressibility and radial stress of the ground when the pile was penetrated downward in a frictional mode. Based on these benefits, the closed form cavity expansion solutions are present to evaluate the skin friction using the stress–dilatancy property and the end bearing capacity inserting the tapering angle. The cylindrical cavity expansion theory evaluates the skin friction together with horizontal (radial) stress when soil particles are displaced with the vertical displacement of piles. The load transfer method iteratively computes the skin friction and horizontal stress for each assumed small segment of the pile from the bottom. Similarly, the spherical cavity expansion theory evaluates the end bearing capacity. Hence, Eq. (2) is used to determine the total bearing capacity, which is further discussed in the following sections along with its detail formulations.

4.1. Analytical model of skin friction

4.1.1. Stress–dilatancy relationship

Davis (1968) assumed that the soil is dilated plastically at a constant rate. The non-associated flow rule is well explained to model dilatants soils that consider the Mohr–Coulomb yield criterion. Generally, a dilatants angle of zero has been considered to compute large strain analyses. In general, the dilatancy angle is considered to be zero for evaluating large strain analyses. However, in reality, the angle of internal friction and the rate of dilatancy at the critical state are interdependent functions of density and effective stress. When a tapered pile penetrates with settlement ratios, the density and confining pressure change significantly. The confining pressure increases with increasing relative density together with the angle of internal friction and dilatancy. The stress–dilatancy property is inserted in the cavity expansion theory proposed by Yu and Houlsby (1991). For the sake of simplicity, an expression explained by Bolton (1986, 1987) is adopted to evaluate the bearing behaviour of different piles. For a plane strain, the following expression can be obtained:

$$\phi'_{\max} - \phi_{cv} = 0.8\psi_{\max} = 5\, I_R^o \tag{3a}$$

$$I_R = I_D(10 - \ln p') - 1 \tag{3b}$$

where $\phi'_{\max}$, ϕ'_{cv}, $\psi_{\max}$, and I_R^o are the maximum angle of friction, the angle of friction at critical states, maximum dilation angle and the relative dilatancy index at plane strain, respectively. The relative dilatancy index I_R is a function of relative density I_D and mean effective stress p' as shown in Eq. (3b). The mean effective stress can be defined as the mean radial and hoop stresses explained in the cavity expansion theory. A plastic zone will be obtained after an initial yielding takes place at the cavity wall within the region $a \le r \le b$, with an increment of cavity pressure p. By partitioning elastic and plastic regions, the meaning of its behaviour can easily be understood. The flow of equations used to determine the cavity pressure is shown in Table 3. Hence, the stress component at the plastic region that satisfies the equilibrium condition can be written as follows:

$$p' = \frac{1}{2}\left[\frac{Y}{\alpha'-1} + Ar^{-\frac{(\alpha'-1)}{\alpha'}} + \frac{Y}{\alpha'-1} + \frac{A}{\alpha'} r^{-\frac{(\alpha'-1)}{\alpha'}}\right] \tag{4a}$$

where p', Y, α', r and A are effective stress, function of cohesion and friction angle, function of cohesion, radius of material point during loading, and constant of integration respectively. Replacing A, the above equation is simplified into the following formula:

$$p' = -p_0 b^{\frac{(\alpha'-1)}{\alpha'}} r^{-\frac{(\alpha'-1)}{\alpha'}} \tag{4b}$$

where p_0 and b are initial cavity pressure and outer radius of the plastic zone during loading. The above Eq. (4b) can be simplified in the elastic–plastic region. At the boundary of the plastic region where $r \le a$, the effective mean stress with the cavity pressure R can be modified as follows:

$$p' = -p_0 R \tag{5}$$

4.1.2. Determination of skin friction

The determination of skin friction is based on τ_x–u_p relationship by dividing the model ground into three stages of pile–ground interaction, such as elastic, elastic until ground starts yielding on slip, and elastic perfectly plastic pile–ground interface during slip. In this section, the deformation behaviours of a compressible elastic pile through differential equations at the equilibrium condition propounded by Kodikara and Moore (1993) are taken into consideration, avoiding the elastic deformation of the steel pile during penetration at a certain depth such that the pile deformation behaviour can be considered as settlement of the pile. Furthermore, the stress–dilatancy property is inserted inside the equation without changing the final results given by Kodikara and Moore (1993).

When the pile–ground interacts, an initial elastic deformation occurs at the first stage. The deformation of the ground is approximated by the theory of concentric cylinder shearing for small tapering angles of 0–5° (Randolph and Wroth, 1978). The settlement of the pile and ground becomes the same when the vertical displacement of the ground, u_g and Poisson's ratio are expressed in terms of the mean radius of the pile r_m. Then, the deformation of pile and ground (τ_x–u_p) relation can be expressed until the pile–ground interface reaches the yield as

$$\tau_x = \frac{G}{\zeta r_m} u_p \tag{6}$$

where G is shear modulus of the ground and ζ is explained in Table 3. At the second stage, the pile–ground interface slips but the ground still demonstrates elastic deformation. In such cases, the vertical pile movement u_p at any point X on the pile–ground interface is greater than the vertical ground movement u_g at the corresponding point Y on the interface. As shown in Fig. 9(a) and (b), the pile is displaced from point X to X' while at the same time, the ground moves from point Y to Y', obtaining the lateral movement (radial expansion) v. For small tapering angles, the increase in radial stress $\Delta\sigma$ for radial

Table 3
Summary of equations used to compute skin friction and end bearing capacity.

A. Equations used to obtain skin friction	Explanations of parameters
$p' = \frac{\sigma_r + \sigma_\theta}{2}$; $\sigma_r = \frac{Y}{\alpha' - 1} + Ar^{-\frac{(\alpha'-1)}{\alpha'}}$; $\sigma_\theta = \frac{Y}{\alpha' - 1} + \frac{A}{\alpha'} r^{-\frac{(\alpha'-1)}{\alpha'}}$ (Yu and Houlsby, 1991)	p' is effective stress, σ_r and σ_θ are radial and hoop stresses; Y is the function of cohesion and friction angle; and α' is the function of cohesion
$\zeta = \ln[2.5L(1-\upsilon)/r_m]$; $\tau_x = (\sigma_0 + \Delta\sigma)\tan(\phi_i + \alpha) + c_i'$; $\Delta\sigma = K_e v$	L is the length of pile, τ_x is average vertical shear stress; σ_0 is initial radial stress; $\Delta\sigma$ is incremental radial stress; ϕ_i is friction angle at interface; and α is tapering angle
$K_p = \frac{1}{A}\frac{1}{C}\frac{\beta+1}{\beta}\left(\frac{a}{a_0}\right)^{(\beta+1)/\beta}\frac{1}{a}$; $= \frac{(\alpha'+1)(\alpha'-1)}{2\alpha'[Y + ((\alpha'-1)\sigma_0)]}$; $C = \frac{-\gamma D R^{-\gamma-1} + \frac{\gamma}{\eta}R^{-\gamma}\frac{d\Lambda(R,\xi)}{dR}}{D^2}$; $D = \left[(1-\delta)^{\frac{(\beta+1)}{\beta}} - \frac{\gamma}{\eta}\Lambda(R,\xi)\right]$	K_p is tangent gradient; A, C and D are constant of integration, α' and β are functions of friction angle and dilation angle; and γ, δ and η are functions of material properties
$\Lambda(R,\xi) = \sum_{n=0}^{n=\infty} P_n$; $P_n = \begin{cases} \frac{\xi^n}{n!}\ln R, & \text{if } n = \gamma. \\ \frac{\xi^n}{n!(n-\gamma)}(R^{n-\gamma} - 1), & \text{otherwise} \end{cases}$ and hence, $\left[\frac{a}{a_0}\right]^{(\beta+1)/\beta} = \frac{R^{-\gamma}}{(1-\delta)^{(\beta+1)/\beta} - \frac{\gamma}{\eta}\Lambda(R,\xi)}$	Λ is infinite power series; ξ is function of material properties; a and a_0 are cavity radius and cavity radius at zero cavity pressure; and n is integer from zero to infinity
B. Equations used to obtain end bearing capacity	**Explanations of parameters**
$K_0 = \frac{1-\sin\phi_\mu'}{1+\sin\phi_\mu'}$; $\sin\phi_{cv}' = \frac{2\sin\phi_\mu'}{1+\sin\phi_\mu'}$; $K_0 = 1 - \sin\phi_{cv}'$ (Ochiai, 1976)	K_0 and ϕ_μ' is the angle of interparticle sliding friction
$q_{pcal} = \frac{3(1+\sin\phi_{cv}')}{(1-\sin(\phi_{cv}'+2\alpha))(3-\sin\phi_{cv}')}[I_{rr}]^{(4\sin\phi_{cv}')/3(1+\sin\phi_{cv}')} \times \left(\frac{1+2K_0}{3}\right)\sigma_v'$	F_q, I_{rr} and I_r are dimensionless spherical cavity expansion factor, reduced rigidity index and rigidity index of soil
$\gamma_{max} = \frac{3p_0\sin\phi_{cv}'}{(3-\sin\phi_{cv}')G}\left(\frac{b}{r}\right)^3 \approx \frac{3p_0\sin\phi_{cv}'}{4G}\left(\frac{b}{r}\right)^3$ (Yamaguchi, 1975) $G = 7.0N^{0.72}$ (MPa) (Yamaguchi, 1975)	p_0, b, r and G are ground stress around the pile tip, radius of plastic zone, radius distance from cavity centre, and shear stiffness
$N = \frac{9I_D^2}{(e_{max}-e_{min})^{1.7}}\left\{\frac{\sigma_v'}{98}\right\}^{0.5}$ (Cubrinosvski and Ishihara, 1999)	I_D, e_{max} and e_{min} are relative density, maximum and minimum void ratios
$G = 7.0\left\{\frac{9I_D^2}{(e_{max}-e_{min})^{1.7}}\left\{\frac{\sigma_v'}{98}\right\}^{0.5}\right\}^{0.72}$; $\Delta_{av} = 50(I_r)^{-1.8}$; $\Delta_{av} = \left\{\frac{\left(\frac{1+2K_0}{3}\right)\sigma'_v\tan\phi'_{cv}}{G}\right\}$	Δ_{av} is average volumetric strain
$q_{pcal} = \frac{A'}{1-\sin(\phi_{cv}'+2\alpha)}\left\{\frac{\frac{G}{\sigma_v'}}{B' + D'\left(\frac{G}{\sigma_v'}\right)^{-0.8}}\right\}^{C'}\sigma_v'$	$A' = \frac{3(1+\sin\phi_{cv}')}{(3-\sin\phi_{cv}')}\left(\frac{1+2K_0}{3}\right)$; $B' = \left(\frac{1+2K_0}{3}\right)\tan\phi_{cv}'$ $C' = \frac{4\sin\phi_{cv}'}{3(1+\sin\phi_{cv}')}$; $D' = 50\left\{\left(\frac{1+2K_0}{3}\right)\tan\phi_{cv}'\right\}^{1.8}$
$q_{cal} = \frac{S/D}{n + m(S/D)}$, Kondner type of hyperbolic	n and m are experimental parameter correspond to the inverse values of initial shear stiffness and an ultimate pile stress

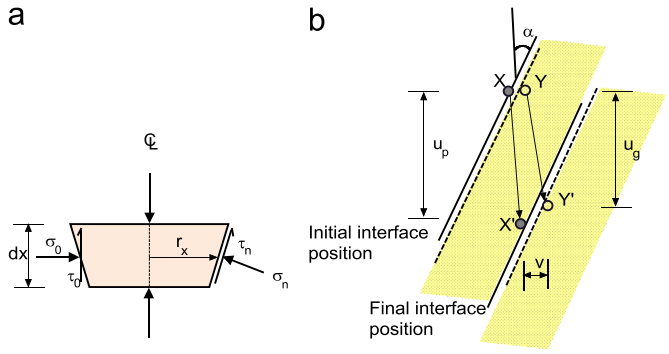

Fig. 9. (a) Segment of pile–ground interface; and (b) kinematics of initial and displaced position.

expansion can be calculated from cylindrical cavity expansion theory and the τ_x–u_p relationship can be expressed in the following terms until the ground starts yielding

$$\tau_x = \frac{K_e \tan\alpha \tan(\phi_i+\alpha)u_p+\sigma_0 \tan(\phi_i+\alpha)+c_i'}{1+\frac{K_e\zeta r_m}{G}\tan\alpha\tan(\phi_i+\alpha)} \quad (7)$$

where

$$K_e = \frac{2G}{r_m}; \quad \text{and} \quad c_i' = \frac{c_i \sec^2\alpha}{(1-\tan\alpha\tan\phi_i)} \quad (7a)$$

At the third stage, when $u_p > (u_p)_Y$ or $\sigma > \sigma_Y$ (where, $(u_p)_Y$ and σ_Y are the pile movement and radial stress at ground yield condition due to expansion) the plastic zone is developed along with slippage to obtain an elastic perfectly plastic pile–ground interface. In this case, the influence of the plastic zone extends further with more pile settlement. It is important to calculate the tangent gradient (K_p) of cavity stress to cavity radius during the expansion given by the solution of Yu and Houlsby (1991). At this stage, a small increment in radial stress ($d\sigma$) can be expressed as

$$d\sigma = K_p dv \quad (8)$$

The radial stress (σ) can be written as

$$\sigma = \sigma_Y + \int_{vY}^{v} K_p dv \quad (9)$$

where v_Y can be computed from (9) using $(u_p)_Y$ and $(\tau_x,)_Y$ which is the vertical shear stress in Eq. (7) when $u_p=(u_p)_Y$. Then, the corresponding vertical shear stress, τ_x can be expressed with the following:

$$\tau_x = \left(\sigma_Y + \int_{vY}^{v} K_p dv\right)\tan(\phi_i+\alpha)+c_i' \quad (10)$$

Eq. (10) measures the skin friction at a certain depth. For a complete pile solution, to activate base and skin resistances, the boundary condition at the base resistance as $x=L$ is assumed to be that of a cylindrical pile. The base resistance can be represented by an elastic spring manner similar to Murff (1989). Following Randolph and Wroth (1978), the base of the pile can be assumed to be similar to a rigid punch

$$\frac{F_b}{(u_p)_b} = \frac{4r_bG}{(1-\nu)\eta_b} \quad (11)$$

where b is the parameter used at the base and η_b is the coefficient introduced to allow for the depth of the pile base below the surface.

4.1.3. Numerical solution and results of the model

The load transfer method proposed by Coyle and Reese (1966) [based on the work of Seed and Reese (1957)] is used to determine the skin friction by inserting a stress–dilatancy property as the extended model of this paper. With this technique, the pile is divided into a number of small segments in order to find the vertical shear stress and horizontal stress along with the pile settlement ratio. During analyses, a small settlement at the pile base is specified and the axial load at the top of this segment is iteratively synchronized to satisfy the equilibrium condition. After obtaining this equilibrium condition, the process undergoes to the next segment and settlements are calculated. All possible functions such as ν, shear modulus, stress–dilatancy properties are successfully calculated by means of iterative techniques. Fig. 10 illustrates a flow chart showing a numerical solution for the proposed extended model and explains the steps of calculation in detail.

The extended model is used to determine the skin friction for various types of soil and pile materials at different relative densities and confining stresses up to 0.4 settlement ratios. The properties of TO sand, K-7 sand and Fanshawe brick sand (FB sand) were taken into consideration. The parameters of FB sand and pile materials were adopted from Sakr et al. (2004, 2005, 2007). Tables 1 and 2 show the fundamental properties of soil and pile materials at different pressures. The pile installation of Fanshawe brick sand was confined to low and high pressures, respectively.

Increases in average vertical shear stresses and radial stresses are clearly shown by Figs. 11 and 12 at different relative densities when different types of model and prototype piles are taken into consideration in order to observe the effect of tapering at different pressures. Increases in the tapering angle serve to increase the stresses for all types of sandy ground and pressures applied in it. Fig. 11 shows that the average vertical shear stresses increased from 2.6 times to 3 times for two different types of soils (TO sand and K-7 sand) with two different relative densities. For instance, TO sand shows a 288% increase in the average vertical shear stress at a 0.1 settlement ratio when compared to straight piles. This percentage further increased to 298% when the pile was penetrated downward up to 0.4 settlement ratio. Similarly, from Fig. 14, it can be noted that at a 0.1 settlement ratio, the radial stress increased by nearly 329% for the maximum angle of tapering at low radial and vertical pressures. When comparing this percentage with high radial and vertical pressures of the same sandy ground (FB sand), the radial stress was found to have increased by up to 339%, which is a difference of 10% between the two different pressures of the same sandy ground. At the mean time, at a 0.4 settlement ratio, both low and high pressures of the sandy ground showed an increase of almost 310% in radial stresses.

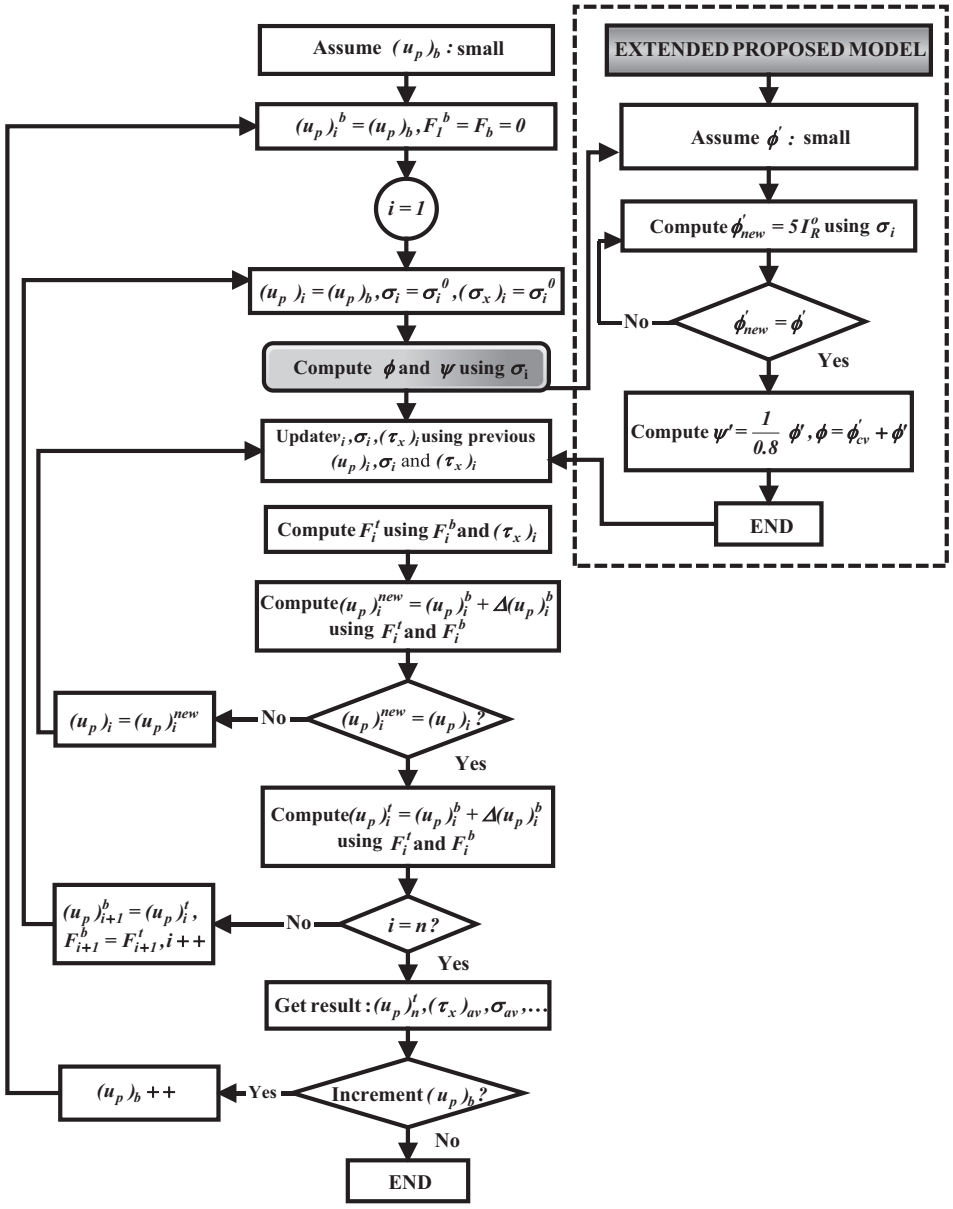

Fig. 10. Flow chart describing the extended model to evaluate skin friction of different types of piles.

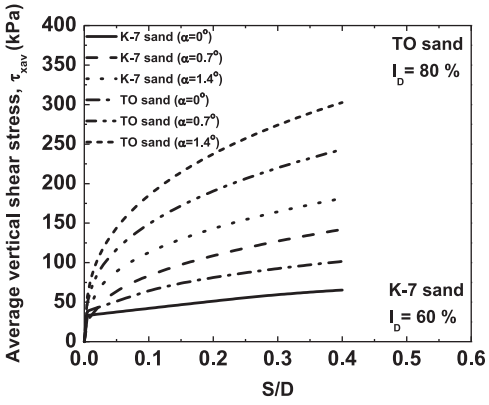

Fig. 11. Average vertical shear stress of K-7 sand and TO sand at different pile tapering angles at normalised settlement ratio.

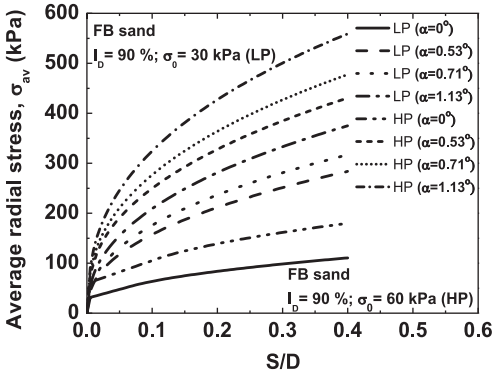

Fig. 12. Average radial stress of FB sand at low and high pressures and different pile tapering angle at normalised settlement ratio.

4.2. End bearing capacity

The pile end bearing capacity in cohesionless soils depends on the compressibility of soil, shear stiffness and strength. Compressibility diverges broadly for different types of soils through incompressible silica sands to highly compressible carbonate sands (Yasufuku et al., 2001). The analytical spherical cavity expansion solution for determination of the end bearing capacity of non-displacement cylindrical pile in closed form was incorporated byYasufuku et al. (1995, 2001). Based on this evaluation technique, the model has been improved to evaluate the end bearing capacity of tapered piles by inserting the tapering factor of the pile. Fig. 13(a) and (b) illustrates the modified failure mechanism which was initially postulated by Yasufuku and Hyde (1995) and Yasufuku et al. (2001) for frictional soils adjunct with cavity expansion pressure p_u proposed by Vesic´,1972 to compute the ultimate bearing capacity q_{pcal}. In the context of the end bearing capacity of tapered piles, it is assumed that the use of cavity expansion theory is a rigid cone of soil that exists beneath the pile tip with the angle ψ' and outside the conical region, the zone is subjected to isotropic stress which is equal to the cavity expansion pressure p_u. Furthermore, there exists an active earth pressure condition σ_A immediately beneath the pile tip along the AC plane. Then, the moment is considered at point B for the cavity expansion pressure p_u, ultimate end-bearing pressure q_{pcal} and the active earth pressure σ_A (Fig. 13). Hence, the ultimate bearing capacity q_{pcal} can be expressed as

$$q_{pcal} = \frac{1}{1-\ \sin\ (\phi_{cv}' + 2\alpha)} p_u \tag{12}$$

For straight piles, the angle of tapering α is zero and Eq. (12) will be reduced in the form $q_{pcal} = 1/(1-\ \sin\ \phi_{cv}'\ )\, p_u$.

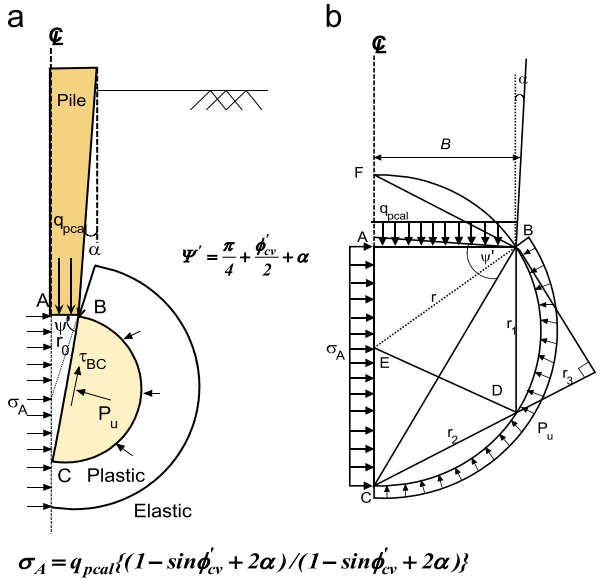

Fig. 13. (a) Concept of modified failure mechanism around the tapered pile tip in cavity expansion solution and (b) geometry of calculation procedure to find ultimate end bearing capacity of tapered pile.

Then, the cavity expansion pressure p_u (Vesic´,1972) becomes

$$p_u = F_q \frac{(1+2K_0)}{3} \sigma_v' \tag{13}$$

where

$$F_q = \frac{3(1+\ \sin\ \phi_{cv}')}{(3-\ \sin\ \phi_{cv}')} [I_{rr}]^{(4\ \sin\ \phi_{cv}')/3(1+\ \sin\ \phi_{cv}')};$$

F_q, I_{rr}, and I_r are related to ϕ', G and Δ_{av} for the plastic zone around a cavity, with the coefficient of earth pressure at rest K_0 and overburden pressure σ_v' (Manandhar and Yasufuku, 2011a, 2011b). Table 3 summarises the computed formulae to evaluate the end bearing capacity of straight and tapered piles.

Using Table 3, the empirically derived reference displacement $(S/D)_{ref}$ for non-displacement soils is expressed as the normalised settlement S/D required to mobilise the half of the ultimate end bearing capacity q_{pcal}, the inverse of the initial shear stiffness is articulated such that

$$n = \frac{\left(\frac{S}{D}\right)_{ref}}{q_{pcal}} \tag{14}$$

where

$$\left(\frac{S}{D}\right)_{ref} = 0.25$$

Rearranging Eq. (14) from Table 3, it can be expressed as follows:

$$q_{cal} = \frac{S/D}{\left(\left(\frac{S}{D}\right)_{ref}/q_{pcal}\right) + \left(\left(\frac{S}{D}\right)/q_{pcal}\right)} = \frac{S/D}{\left\{0.25 + \frac{S}{D}\right\}} q_{pcal} \tag{15}$$

The applied pile tip stress at any pile tip settlement can be calculated using only three parameters needed for calculating the q_{pcal} in Eq. (15), which presents the effects of the overburden pressure, soil compressibility, shear stiffness and strength of soil. This indicates that the load–settlement curves can easily be computed from the fundamental in-situ soil data. The total end bearing capacity is calculated as

$$P_B = q_{cal}\, \pi {r_b}^2 \tag{16}$$

where r_b is the radius of the pile tip.

In the closed form cavity expansion theory, the total end bearing capacity increases in line with increases to the tapering angle. When different radial stresses are furnished at the same density ground, high radial stresses govern the higher end bearing capacity in FB sand, as shown in Fig. 14.

The proposed model can evaluate the tapering effects at a critical state condition when the ultimate bearing capacity is normalised with the cavity pressure. Fig. 15 shows the relationship between normalised ultimate bearing capacity and the angle of friction at the critical state for different types of tapering angles. Increasing the tapering angle causes the normalised ultimate bearing capacity to increase. At the same time, increasing the critical state friction angle also causes the normalised ultimate bearing capacity to increase.

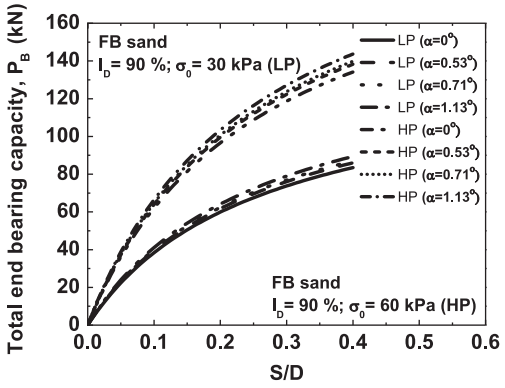

Fig. 14. Total end bearing capacity of FB sand of different piles at normalised settlement ratio.

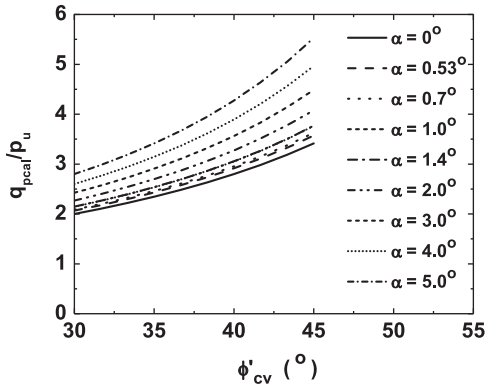

Fig. 15. Normalised ultimate bearing capacity of tapered piles at critical state condition.

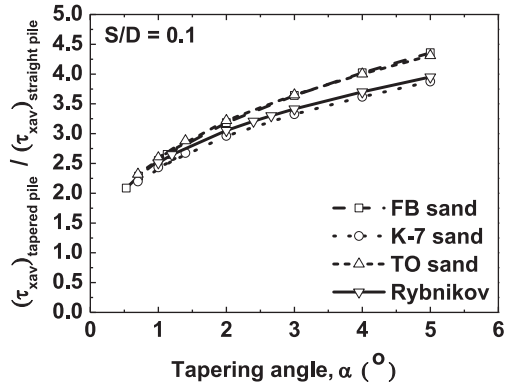

Fig. 16. Effect of angle of tapering on normalised average vertical shear stress.

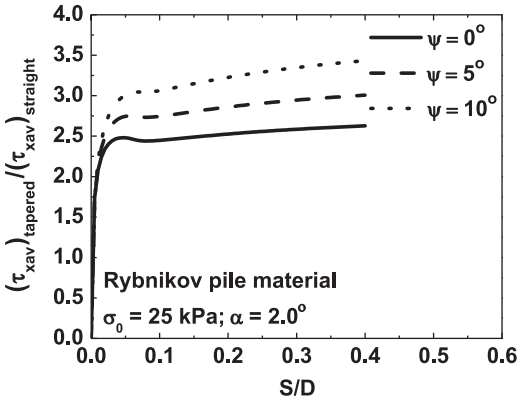

Fig. 17. Effects of dilatancy angle on normalised average vertical shear stress.

5. Applicability of the extended model to evaluate total bearing capacity

A real type Rybnikov (1990) pile and prototype pile (Sakr et al., 2004, 2005, 2007) are adopted to check and validate the applicability of the proposed model. Rybnikov (1990) carried out tests in the Irtysh Pavlodar region of the former Soviet Union and used bored-cast-in-place tapered piles. Seven different types of piles were accomplished, each having a length of 4.5 m, constituting five tapered piles and two cylindrical piles in order to understand the behaviour of tapered piles. The top and bottom radii of piles were 200 mm and 100 mm (1.2°): one tapered pile with a corresponding radii of 250 mm and 100 mm (2°) and two tapered piles had radii of 300 mm and 100 mm (2.4°), respectively. Here, the soil parameters of TO sand (Table 2) were used for analyses. Fig. 16 shows the effect of tapering angle for all types of soil and pile materials used by taking the ratios of the average vertical shear stress of tapered piles to that of straight piles. The parametric study shows that the average vertical shear stress increased in the most tapered pile on FB sand by 236%. Similarly, for K-7 sand and Rybnikov pile, it shows an increase of 331% and 287%, respectively. Proceeding on from this, Fig. 17 shows the effect of dilatancy property by the Rybnikov pile material for evaluating the side resistance. At a 0.1 settlement ratio, the normalised side resistance increased by up to 30% for a dilation angle of 5° and 61% for a dilation angle of 10° compared to dilation angle of zero (at a critical state condition). When the effect was examined at 0.4 settlement ratios, it was increased up to 38% for a 5° dilation angle and 81% for a 10° dilation angle.

Moreover, measured experimental pile loading data and predicted data of Sakr et al. (2004, 2005, 2007) were compared at low and high pressures with tapering angles of 0.71° and 1.13°. Figs. 18 and 19 show the measured and predicted skin friction with respect to settlement ratios. At low settlement ratios, the values of measured and predicted skin frictions lie near to each other. When increasing the settlement ratio, low pressure data in Fig. 18(a) shows it was slightly underestimated, being below the measured data at different 1.13° tapering for Fanshawe brick sand of the prototype test. At the mean time, at high pressures as shown by Fig. 18(b), the measured data for relatively low angle of tapering of 0.73° was slightly overestimated. Similarly, when observed in model tests (Fig. 19) for Toyoura sand, the predicted results are quite near. In general, it is noticed that with the increase in the degree of tapering and settlement ratios, skin friction also increases by following similar trends as straight piles.

The validity of the extended model was checked after comparing measured and predicted results together with parametric studies on real type, prototype and model tests using Tables 1 and 2. Fig. 20 denotes the validity of unit skin

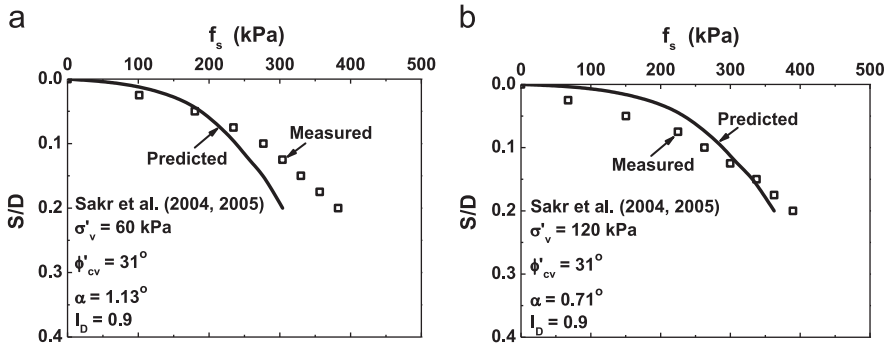

Fig. 18. Measured and predicted skin friction of FB sand at (a) low pressure high tapering angle and (b) high pressure low tapering angle.

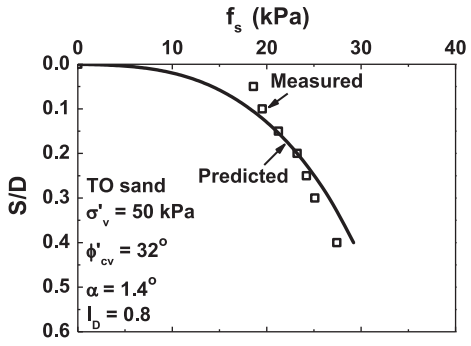

Fig. 19. Measured and predicted skin friction of TO sand at high tapering angle.

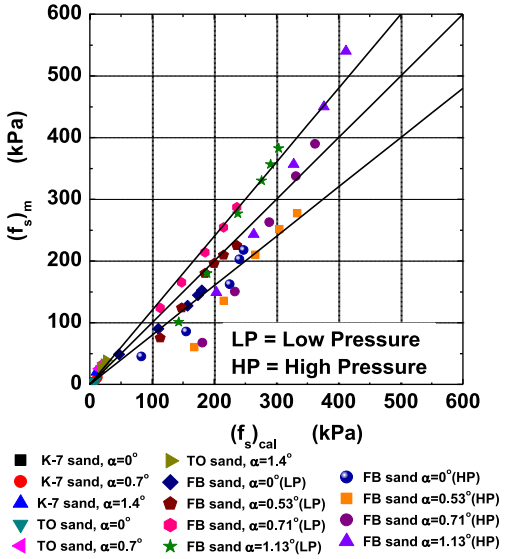

Fig. 20. Prediction of calculated and measured skin friction at different relative densities and pressures.

frictions of measured and calculated data. The extended model shows the consistent agreement between measured and calculated unit skin frictions for different types of piles and sandy ground.

The proposed model for evaluating end bearing capacity was checked with measured data with various source paper using Table 4. Additional data of BCP (1B) (1971) (BCP Committee, 1971) and Yasufuku et al. (2001) were used to check with the predicted end bearing capacity on straight cylindrical piles. In this paper, if tapered piles are used in these locations using the same soil properties, the expected end bearing capacities can be predicted in the real field. In this regard, Fig. 21(a)–(d) shows the expected end bearing capacities for all types of pile and soil materials, which show good increasing trends with increasing tapering angles when penetrating downward in a frictional mode.

Moreover, these additional source data along with BCP (5C) (1971), Japan Geotechnical Society (JGS) (1993), prototype tests by Sakr et al. (2004, 2005, 2007) and smaller model tests were plotted. Fig. 22 shows a remarkable similarity with the proposed model at a 1:1 ratio. The proposed model proves the tapering effects of end bearing capacity during the pile penetration.

Recalling Eq. (1) and Fig. 1, the total bearing capacity is the summation of the total skin friction around the shaft and pile tip bearing capacity. Using Eq. (2) in the above section, the total bearing capacity of different piles on different types of soils can be determined. Fig. 23 represents an example of evaluating the total bearing capacity of the prototype test. Increasing the tapering angle serves to increase the total bearing capacities at low and high pressures, respectively. Fig. 24 shows that the total bearing capacity of tapered piles in FB sand supports the proposed models. There is an ideal match with the total capacity of prototype FB sand and its corresponding pile material at a 0.1 settlement ratio measured in kN. The predicted ratios of FC, T3, T4, and T5 at low pressure are 1.19, 0.96, 0.97 and 0.94, respectively. At the same time, the predicted ratios at high pressure are 0.98, 1.01, 1.10 and 1.15, respectively.

6. Concluding remarks

The mobilised mechanism of skin friction and end bearing capacity through the smallest model pile load testing shows that the effective radius of the influenced zone around the pile shaft increases in line with increases in the tapering angle. A visual inspection confirmed that the narrowing of the convex heave on the pile–ground interface was due to an increase in radial stress by the tapered pile. In the meantime, the effective length of the failure tip increases in line with increases to the

Table 4
Pile geometry and soil characteristics from different source papers.

Source paper	No.	Pile geometry		Soil characteristics			
		Dia., d (m)	Length, L (m)	Soil type	σ'_v (kPa)	$\phi'_{cv,\ av}$ (deg)	N_{av} (G) (MPa)
BCP (1B) (BCP Committee, 1971)	1	0.2	4	Fine sand	60	35 (34–36)	20 (60.5)
BCP (1B) (BCP Committee, 1971)	2	0.2	11	Dense sand	170	37 (36–38)	48 (133.5)
JGS data (1993)	3	1.5	44.5	Sand	300	35	25 (71.1)
	4	1.5	32	Sand	356	(34–36)	30 (81)
	5	1.5	26.5	Sand	256	35	30 (81)
	6	1.5	22.4	Sand	212	(34–36)	30 (81)
Yasufuku et al. (2001)	7	0.03	–	Quiou sand	100	36	– (21.9)
	8				200		– (42)
	9				400		– (47.0)

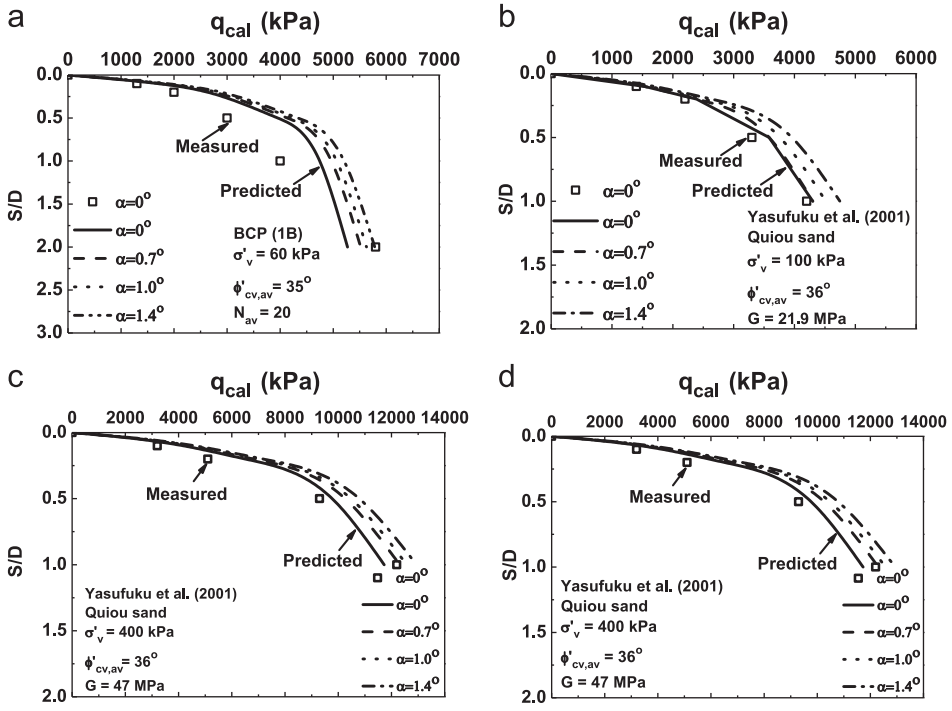

Fig. 21. Measured, predicted and expected end bearing capacity of different piles: (a) source from BCP (1B), (b–d) Yasufuku et al. (2001) at different confining pressures.

tapered pile. In addition, the relatively larger model test shows that the increase in normalised radial distance of tapered piles (0–1.4°) affects at least three times nearer the pile–ground interface by the most tapered pile compared to cylindrical straight pile, which indicates the increase in radial stresses of the ground. Based on these benefits of tapered piles, two analytical models were present to evaluate the skin friction and end bearing capacity separately. Their applications have been verified using model tests, prototype tests, and a real type database. The main important conclusions can be addressed as follows:

(1) The extended model with the inserted stress–dilatancy property can predict skin friction using cylindrical cavity expansion theory in closed form solutions. The dilatancy index can smoothly evaluate the skin friction of tapered piles at any confining pressure irrespective of the type of sand.
(2) The insertion of tapering angle to the spherical cavity expansion theory predicts the end bearing capacity of tapered piles. When the critical state friction angle is increased, the ultimate bearing capacity normalised by cavity pressure also increases in line with increases to the tapering angle of piles.
(3) The closed form solution has the practical advantage of evaluating skin friction and end bearing capacity in a simple way. The pile load–settlement curves can easily be determined with the aid of the simple fundamental properties of soils.
(4) The predicted skin friction using the extended model shows good and reliable trend with measured skin friction.

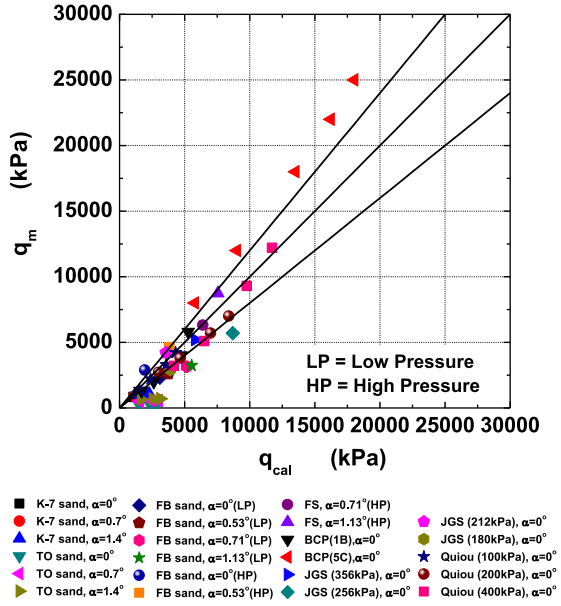

Fig. 22. Prediction of calculated and measured end bearing capacity of model and prototype tests.

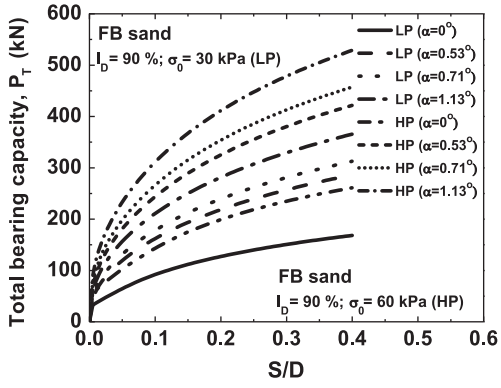

Fig. 23. Total bearing capacity of prototype test.

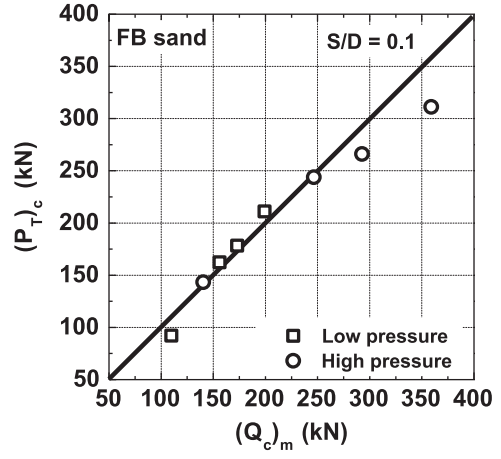

Fig. 24. Ideal prediction of calculated and measured total capacity of prototype pile at 0.1 settlement ratio.

Similarly, the expected end bearing capacity shows remarkably good tendencies compared with the measured end bearing capacity of cylindrical straight piles.

(5) The measured and calculated unit skin friction and end bearing capacity from various sources at different soil types and tapering angles at different relative densities show consistent agreement with each other. This indicates the ability of the model to evaluate the bearing behaviour of tapered piles in any type of sandy ground. When the total capacity of the measured prototype test database is compared with the calculated ones at different pressures, they ideally fit with each other.

Acknowledgements

The authors would like to express their heartfelt thanks to Professor Kiyoshi Omine, laboratory assistant Mr. Michio Nakashima and colleague Mr. Tohio Ishimoto for their invaluable support in carrying out this research.

References

Baligh, M.M., 1976. Cavity expansion in sands with curved envelopes. J. Geotech. Eng.: ASCE 102 (GT11), 1131–1145.

BCP Committee, 1971. Field tests on piles in sand. Soils Found. 11 (2), 29–50.

Bolton, M.D., 1986. The strength and dilatancy of sands. Géotechnique 36 (1), 65–78.

Bolton, M.D., 1987. Discussion on the strength and dilatancy of Sands. Géotechnique 37 (2), 219–226.

Coyle, H.M., Reese, L.C., 1966. Load transfer for axially loaded piles in clay. Int. J. Soil Mech. Found. Div.: ASCE 92 (1), 1–26.

Cubrinosvski, M., Ishihara, K., 1999. Empirical correlation between SPT *N*-value and relative density for sandy soils. Soils Found. 39 (5), 61–71.

Davis, E.H., 1968. Theories of plasticity and the failure of soil masses. Selected topics. In: Lee, I.K. (Ed.), Soil Mechanics. Butterworths, London, UK., pp. 341–380.

Dmokhovskii, V.K., 1927. Effect of geometric shape of pile on its penetration resistance. Trans. Moscow Inst. Railroad Transp. Eng. (MIIT) VI (in Russian).

Horvath, J.S., Trochalides, T., 2004. A half century of tapered pile usage at the John F. Kennedy International Airport. In: Proceedings of the Fifth Case History Conference on Geotechnical Engineering. New York, NY, USA, Paper no. 11-02.

Hughes, J.M.O., Wroth, C.P., Windle, D., 1977. Pressuremeter tests in sands. Geotechnique 27 (4), 455–477.

Japan Geotechnical Society, 1993. JGS standard for vertical load tests of piles. J. Geotech. Soc., 151–206 (in Japanese).

Japan Geotechnical Society 0161-2009, 2009. Test methods for minimum and maximum densities of sands. Laboratory Testing Standards of Geomaterials. pp. 195–198 (in Japanese).

Kézdi, A., 1975. Pile foundations. In: Winterkorn, H.F., Fang, H.Y. (Eds.), Foundation Engineering Handbook first ed. Van Nostrand Reinhold, New York, pp. 550–600.

Kodikara, J.K., Moore, I.D., 1993. Axial response of tapered piles in cohesive frictional ground. J. Geotech.l Eng.: ASCE 119, 675–693.

Manandhar, S., Yasufuku, N., Shomura, K., 2009a. Skin Friction of taper-shaped piles in sands. In: Proceedings of the 28th ASME International Conference on Ocean, Offshore and Arctic Engineering (OMAE). Honolulu, Hawaii, USA, pp. 93–102.

Manandhar, S., Yasufuku N., Omine K., Qiang, L., 2009b. Mobilized mechanism of skin friction of tapered piles in sand. In: Proceedings of

the International Joint Symposium on Geo-Disaster Prevention and Geoenvironment in Asia-JS-Fukuoka 2009. Fukuoka, Japan, pp. 171–178.
Manandhar, S., 2010. Bearing capacity of tapered piles in sands (Ph.D. Thesis), Kyushu University, (unpublished).
Manandhar, S., Yasufuku N., Omine, K., 2010a. Tapering effects of piles in cohesionless soil. In: Proceedings of the 4th Japan–China Geotechnical Symposium on Recent Developments of Geotechnical Engineering. Okinawa, Japan, pp. 477–482.
Manandhar, S., Yasufuku, N., Omine, K., Taizo, K., 2010b. Response of tapered piles in cohesionless soil based on model tests. J. Nepal Geol. Soc. 40, 85–92.
Manandhar, S., Yasufuku, N., 2011a. End bearing capacity of tapered piles in sands using cavity expansion theory. Mem. Fac. Eng. Kyushu Univ. 71 (4), 77–99.
Manandhar, S., Yasufuku, N., 2011b. Evaluation of skin friction of tapered piles in sands based on cavity expansion theory. Mem. Fac. Eng. Kyushu Univ. 71 (4), 101–126.
Miura, S., Toki, S., 1982. A sample preparation method and its effect on static and cyclic deformation–strength properties of sand. Soils Found.—Japan. Geotech. Soc. 22 (1), 62–77.
Murff, J.D., 1989. Response of axially loaded piles. J. Geotech. Eng.: ASCE 101 (3), 356–360.
Norlund, R.L., 1963. Bearing capacity of piles in cohesionless soils. J. Soil Mech. Found.: ASCE 117 (8), 1208–1226.
Ochiai, H., 1976. The coefficient of earth pressure at rest of sands. Soils Found. 16 (2), 105–111 (in Japanese).
Randolph, M.F., Wroth, C.P., 1978. Analyses of deformation of vertically loaded piles. J. Geotech. Eng.: ASCE 104 (12), 1465–1488.
Rybnikov, A.M., 1990. Experimental investigation of bearing capacity of bored-cast-in-place tapered piles. Soil Mech. Found. Eng. 27 (2), 48–52.
Sakr, M., El Naggar, M.H., Nehdi, M.L., 2004. Load transfer of fibre-reinforced polymer (FRP) composite tapered piles in dense sand. Can. Geotech. J. 41 (1), 70–88.
Sakr, M., El Naggar, M.H., Nehdi, M.L., 2005. Uplift performance of FRP tapered piles in dense sand. IJPMG—Int. J. Phys. Modelling Geotech. 2, 1–16.
Sakr, M., El Naggar, M.H., Nehdi, M.L., 2007. Wave equation analyses of tapered FRP-concrete piles in dense sand. Soil Dyn. Earthquake Eng. 27, 166–182.
Seed, H.B., Reese, L.C., 1957. The action of soft clay on friction piles. Trans. ASCE 122, 731–754.
Vesic‘, A.S., 1972. Expansions of cavities in infinite soil mass. J. Soil Mech. Found. Eng.: ASCE 98 (SM3), 265–290.
Yamaguchi, H., 1975. Pile end-bearing capacity based on an elasto-plastic analysis and its application. Tsuchi-to-Kiso JGS Ser. 209 23 (7), 7–11 (in Japanese).
Yasufuku, N., Hyde, A.F.L., 1995. Pile end-bearing capacity in crushable sands. Géotechnique 45 (4), 663–676.
Yasufuku, N., Ochiai, H., Maeda, Y., 1995. Geotechnical analysis of skin friction of cast-in-place piles related to critical state friction angle. J. Geotech. Eng. JSCE 617 (III-46), 89–100 (in Japanese).
Yasufuku, N., Ochia, H., Ohno, S., 2001. Pile end-bearing capacity of sand related to soil compressibility. Soils Found.—Japan. Geotech. Soc. 41 (4), 59–71.
Yu, H.S., Houlsby, G., 1991. Finite cavity expansion in dilatants soils: Part 1. Loading analysis. Géotechnique 41 (2), 173–183.